UPLIFT OF THE ANTARCTIC CONTINENT IN ELASTIC DEFORMATION

Katsutada KAMINUMA,

National Institute of Polar Research, 9–10, Kaga 1-chome, Itabashi-ku, Tokyo 173

Ryosuke SATO,

Yasunori SUZUKI

and

Mitsuhiro MATSU'URA

Geophysical Institute, Faculty of Science, University of Tokyo, Yayoi 2-chome, Bunkyo-ku, Tokyo 113

Abstract: The uplift of the shorelines in snow-free areas of the Antarctic Continent is estimated to be 20–30 m and the retreat of the ice sheet to be 10–100 km. This paper tries a theoretical interpretation of this uplift in terms of static deformation of an elastic semi-infinite medium or multi-layered medium due to the diminution of the load on the surface. As the forms of load function, which can be regarded as almost the same as the form of the ice sheet, two types of functions are considered as follows: Case I where constant pressure acts on the surface within a circular area, and Case II where pressure varies with the radius of a circular. As the crust and mantle structures, three models (Semi-infinite A, Semi-infinite B, and CANSD) are considered.

The uplift is calculated by the difference in vertical displacements between the initial and the final states of the ice sheet. The initial thickness and the radius of ice sheet are denoted by H and a, and the decreases in thickness and radius are denoted by ΔH and Δa, respectively. The observed uplift can be explained by the following either set of H and ΔH with fixed a ($=1700$ km) and Δa ($=50$ km) for the Semi-infinite B and the CANSD models; for Case I, $H=2.0$ km and $\Delta H=0$–0.1 km, and for Case II, $H=4.0$ km and $\Delta H=0$–0.1 km. Reasonable values of H and ΔH are not obtained for the Semi-infinite A model for both Cases I and II.

1. Introduction

Because of some fossils of plants and animals found in the Antarctic, it is considered that the Antarctic Continent had a warm climate and snow-free areas before Mesozoic era. It is known, however, that for the last 4 million years the continent has been covered by thick ice sheet and that the ice sheet on East Antarctica in the

Tertiary period was much thicker than the present. At present 90% of ice on the earth is found on and around the Antarctic Continent, and more than 95% of this continent is covered by the ice sheet with the mean thickness of 1.9 km. Antarctica is the only one continent on the earth covered by the ice sheet all the year round. It is one of important problems in the solid earth geophysics to investigate the effect of huge ice sheet on the topography and properties of the crust and mantle of the Antarctic Continent.

It is known from geomorphological data that the ice sheet on Antarctica has repeated advance and retreat in the past several ten million years at least and the ice sheet has retreated in the last ten thousand years. The land uplift due to this retreat is observed on the shorelines of snow-free areas.

This paper tries to elucidate the uplift by simple models. Surface deformation is computed in the case of simple loading on a confined area of the surface of a semi-infinite or a multi-layered medium. Taking into account the very long time scale of the crustal deformation of the Antarctic Continent, it will be enough to consider the static deformation due to the retreat of the ice sheet.

2. Surface Displacement of a Multi-layered Medium

In this section, we consider a medium composed of n parallel, homogeneous layers overlying an elastic half space. We take a cylindrical coordinate system (r, φ, z), the origin being located on the uppermost free surface, and the vertical z-axis pointing downward into the half space. The geometry and notations are shown in Fig. 1. SATO (1971) treated the problem of static deformation due to a fault in a multi-layered medium. Following that method, the expressions of surface displacements due to the axially symmetric load can be obtained. We here report the final results, presenting the definitions of some functions in the Appendix.

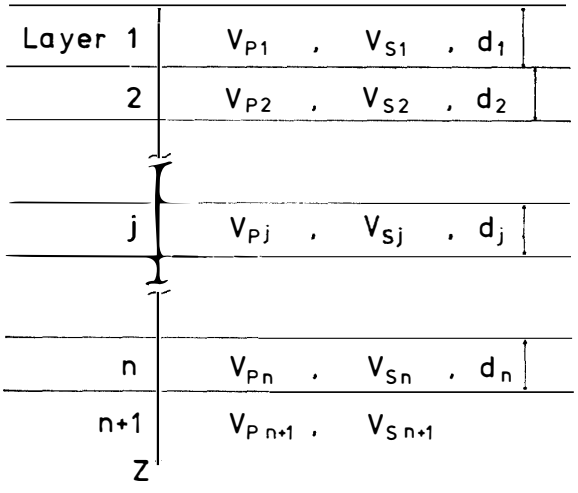

Fig. 1. Geometry and notations for a multi-layered medium.
$V_{pj}=\sqrt{(\lambda_j+2\mu_j)/\rho_j}$; P wave velocity of the j-th layer
$V_{sj}=\sqrt{\mu_j/\rho_j}$; S wave velocity of the j-th layer
λ_j, μ_j; Lamé's elastic constants of the j-th layer
ρ_j; density of the j-th layer
d_j; thickness of the j-th layer

Integral representations of the surface displacements are given by

$$U_r=u_r(z=0)=-\frac{1}{2\mu_1}\int_0^\infty K_r(\xi)W^*(\xi)J_1(\xi r)d\xi,$$
$$U_z=u_z(z=0)=\frac{1}{2\mu_1}\int_0^\infty K_z(\xi)W^*(\xi)J_0(\xi r)d\xi, \tag{1}$$

where $W^*(\xi)$ is the Hankel transform of order zero of the load function $W(r)$, that is,

$$W^*(\xi)=\int_0^\infty W(r)J_0(\xi r)rdr,$$
$$W(r)=\int_0^\infty W^*(\xi)J_0(\xi r)\xi d\xi, \tag{2}$$

and $J_0(\xi r)$ and $J_1(\xi r)$ are the Bessel functions of order zero and one, respectively.

The definitions of $K_r(\xi)$ and $K_z(\xi)$ are given in the Appendix, where it is shown that K_r and K_z for a semi-infinite medium reduce to $(1-\alpha_1)/\alpha_1$ and $1/\alpha_1$, respectively.

To evaluate the semi-infinite integrals in eq. (1), approximations of the functions $K_r(\xi)$ and $K_z(\xi)$ by some integrable functions are necessary for accomplishing integrations in an analytical way. Such a technique of evaluating the integrals has also been used in a series of the works treating static deformations due to a fault in a multilayered medium (SATO, 1971; SATO and MATSU'URA, 1973; MATSU'URA and SATO, 1975), in which detailed discussions on the technique and its validity are given. In the present study, the following types of functions, $F_{r(\mathrm{or}\,z)}(\xi)$, are taken as the approximation functions for $K_{r(\mathrm{or}\,z)}(\xi)$ respectively.

$$F_r(\xi)=a_r+b_r\xi^{c_r},$$
$$F_z(\xi)=a_z+b_z\xi^{c_z}, \tag{3}$$
$$0<c_r<1,\quad 0<c_z<1.$$

These functions are much simpler than those adopted in the study on strain and tilt, such as

$$a_{r(\mathrm{or}\,z)}+b_{r(\mathrm{or}\,z)}\xi+c_{r(\mathrm{or}\,z)}e^{-k_{1r(\mathrm{or}\,z)}\xi}+d_{r(\mathrm{or}\,z)}e^{-k_{2r(\mathrm{or}\,z)}\xi}, \tag{4}$$

(MATSU'URA and SATO, 1975), but both of the results calculated from these different types of the approximation functions coincide with each other with a sufficient accuracy in the present structure model described later.

The final expressions of the surface displacements reduced from eq. (1) by using the approximation function $F_{r(\mathrm{or}\,z)}(\xi)$ in eq. (3) are shown for two special cases.

$$\text{Case I;}\quad W(r)=\begin{cases}W_0, & 0\leqq r<a\\ 0\ , & a<r.\end{cases} \tag{5}$$

Replacing the variable r by a normalized one $s(=r/a)$, and the coefficients c_r and c_z in eq. (3) by t and t' respectively, the surface displacements are written as

$$\left.\begin{aligned} U_r(s)&=-\frac{W_0 a}{2\mu_1}(a_r I_{r1}+b_r I_{r2}),\\ U_z(s)&=\frac{W_0 a}{2\mu_1}(a_z I_{z1}+b_z I_{z2}), \end{aligned}\right\} \tag{6}$$

with

$$I_{r1}=\begin{cases} \dfrac{s}{2}, & 0\leq s\leq 1,\\ \dfrac{1}{2s}, & 1<s, \end{cases} \tag{7}$$

$$I_{z1}=\begin{cases} F\left(\dfrac{1}{2}, -\dfrac{1}{2}, 1; s^2\right), & 0\leq s\leq 1,\\ \dfrac{1}{2s}F\left(\dfrac{1}{2}, \dfrac{1}{2}, 2; \dfrac{1}{s^2}\right), & 1<s, \end{cases} \tag{8}$$

$$I_{r2}=\begin{cases} \dfrac{2^t\Gamma(t/2)}{\Gamma(1-t/2)}\dfrac{t}{4}sF\left(1+\dfrac{t}{2}, \dfrac{t}{2}, 2; s^2\right), & 0\leq s\leq 1,\\ \dfrac{2^t\Gamma(t/2)}{\Gamma(1-t/2)}\dfrac{t}{4}\dfrac{1}{s^{1+t}}\Gamma\left(1+\dfrac{t}{2}, \dfrac{t}{2}, 2; \dfrac{1}{s^2}\right), & 1<s, \end{cases} \tag{9}$$

$$I_{z2}=\begin{cases} \dfrac{2^{t'}\Gamma((1+t')/2)}{(1-t')\Gamma((1-t')/2)}F\left(\dfrac{1+t'}{2}, \dfrac{t'-1}{2}, 1; s^2\right), & 0\leq s\leq 1,\\ \dfrac{2^{t'}\Gamma((1+t')/2)}{(1-t')\Gamma((1-t')/2)}\dfrac{1}{s^{1+t'}}F\left(\dfrac{1+t'}{2}, \dfrac{1+t'}{2}, 2; \dfrac{1}{s^2}\right), & 1<s, \end{cases} \tag{10}$$

where $\Gamma(z)$ and $F(\alpha, \beta, \gamma; z)$ are the Gamma-function and the Gauss' hypergeometric function, respectively.

$$\text{Case II;}\quad W(r)=\begin{cases} W_0\sqrt{1-(r/a)^2}, & 0\leq r\leq a,\\ 0, & a<r. \end{cases} \tag{11}$$

For this case, the expressions of the surface displacements are

$$\left.\begin{aligned} U_r(s)&=-\frac{W_0 a}{2\mu_1}\sqrt{\frac{\pi}{2}}(a_r I_{r1}+b_r I_{r2}),\\ U_z(s)&=\frac{W_0 a}{2\mu_1}\sqrt{\frac{\pi}{2}}(a_z I_{z1}+b_z I_{z2}), \end{aligned}\right\} \tag{12}$$

with

$$I_{r1}=\begin{cases} \sqrt{\dfrac{2}{\pi}}\dfrac{1}{3s}[1-(1-s^2)^{3/2}], & 0\leq s\leq 1,\\ \sqrt{\dfrac{2}{\pi}}\dfrac{1}{3s}, & 1<s, \end{cases} \tag{13}$$

$$I_{z1}=\begin{cases}\dfrac{1}{2}\sqrt{\dfrac{\pi}{2}}\left(1-\dfrac{s^2}{2}\right), & 0\leq s\leq 1\\ \dfrac{1}{4}\sqrt{\dfrac{2}{\pi}}s\left[\left(1-\dfrac{1}{s^2}\right)^{1/2}-s\left(1-\dfrac{1}{s^2}\right)\sin^{-1}\left(\dfrac{1}{s}\right)\right], & 1<s,\end{cases} \tag{14}$$

$$I_{r2}=\begin{cases}\dfrac{1}{2\sqrt{2}}\dfrac{2^t\Gamma(t/2)}{\Gamma((1-t)/2)}\dfrac{t}{(1-t)}sF\left(1+\dfrac{t}{2},-\dfrac{1-t}{2},2;s^2\right), & 0\leq s\leq 1,\\ \dfrac{1}{3\sqrt{2\pi}}\dfrac{2^t\Gamma(t/2)}{\Gamma(1-t/2)}t\dfrac{1}{s^{t+1}}F\left(1+\dfrac{t}{2},\dfrac{t}{2},\dfrac{5}{2};\dfrac{1}{s^2}\right), & 0<s,\end{cases} \tag{15}$$

$$I_{z2}=\begin{cases}\dfrac{1}{\sqrt{2}}\dfrac{2^{t'}\Gamma((1+t')/2)}{\Gamma(1-t'/2)}\dfrac{1}{(2-t')}F\left(\dfrac{1+t'}{2},-\left(1-\dfrac{t'}{2}\right),1;s^2\right), & 0\leq s\leq 1,\\ \dfrac{1}{3}\sqrt{\dfrac{2}{\pi}}\dfrac{2^{t'}\Gamma((1+t')/2)}{\Gamma((1-t')/2)}\dfrac{1}{s^{1+t'}}F\left(\dfrac{1+t'}{2},\dfrac{1+t'}{2},\dfrac{5}{2};\dfrac{1}{s^2}\right), & 1<s,\end{cases} \tag{16}$$

where the quantities s, t, and t' are the same as those in the Case I. The evaluations of $\Gamma(z)$ and $F(\alpha, \beta, \gamma; z)$ can be numerically done by using a high-speed computer.

As already stated, $K_r(\xi)$ and $K_z(\xi)$ for a semi-infinite medium reduce to $(1-\alpha_1)/\alpha_1$ and $1/\alpha_1$ respectively. And we can get the surface displacements in eqs. (6) and (12) by setting

$$a_r=(1-\alpha_1)/\alpha_1, \quad a_z=1/\alpha_1, \quad b_r=b_z=c_r=c_z=0. \tag{17}$$

3. Numerical Results

The equations obtained in the previous section are used to calculate the surface displacements. Since only the data on vertical uplift of the surface of the Antarctic Continent is available, we consider mainly the vertical displacement U_z.

If $W(r)$ in the equations is assumed to be due to the ice sheet on the continent, the constant factor W_0 may be expressed by $W_0=\rho gH$, where ρ is the density of ice, g the gravitational acceleration, and H the thickness of ice sheet. In Case II, H is taken as the largest thickness of the ice sheet, *i. e.*, the thickness at the center ($r=0$) of the ice sheet.

As the details of the crust and mantle structure beneath Antarctica are not known as yet, for the present multi-layered model, we adopt the model for the Canadian Shield (CANSD model) proposed by BRUNE and DORMAN (1963); the CANSD model seems to be sufficient to represent the structure beneath the Antarctic Continent for the present study. The parameters of the CANSD model are listed in Table 1. For the parameters of the semi-infinite medium, two models are considered. The first, which hereafter we refer to as Semi-infinite A, is that with the same parameters as those in the third layer of the CANSD model. The other, which we call Semi-infinite B, is that with parameters which are the thickness-weighted-mean for the upper seven layers of the CANSD model. The parameters of the semi-infinite media

Table 1. CANSD model by BRUNE and DORMAN (1963).

j layer number	d_j(km) layer thickness	V_{pj}(km/s) P-wave velocity	V_{sj}(km/s) S-wave velocity	ρ_j(g/cm^3) density
1	6.0	5.64	3.47	2.70
2	10.5	6.15	3.64	2.80
3	18.7	6.60	3.85	2.85
4	80.0	8.10	4.72	3.30
5	100.0	8.20	4.54	3.44
6	100.0	8.30	4.51	3.53
7	80.0	8.70	4.76	3.60
8	∞	9.30	5.12	3.76

Table 2. Semi-infinite media A and B used in this study.

	V_p(km/s)	V_s(km/s)	ρ(g/cm^3)
A	6.60	3.85	2.85
B	8.08	4.52	3.41

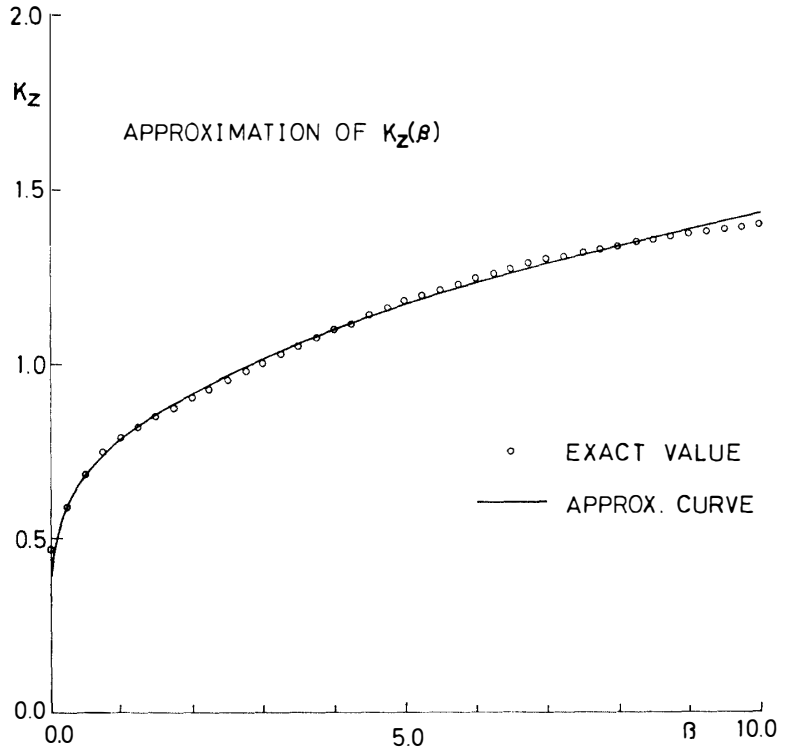

Fig. 2. Approximation function $F_z(\beta)$ for $K_z(\beta)$ (solid curve). Exact values of $K_z(\beta)$ are shown by open circles. $\beta=\xi a$ is a nondimensionalized wave number.

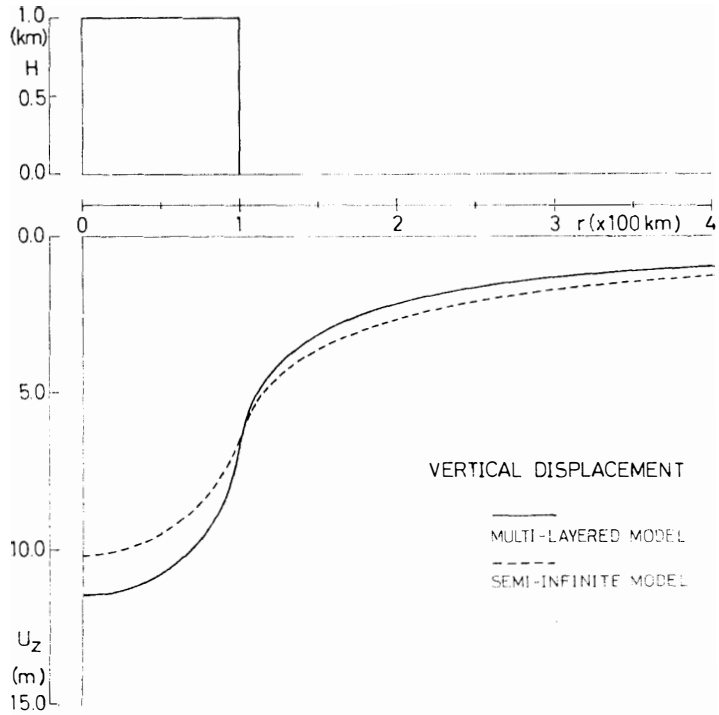

Fig. 3. Vertical displacements of the surface of the CANSD model (solid curve) and of Semi-infinite B (broken curve) for the Case I load with H = 1 km and a = 100 km.

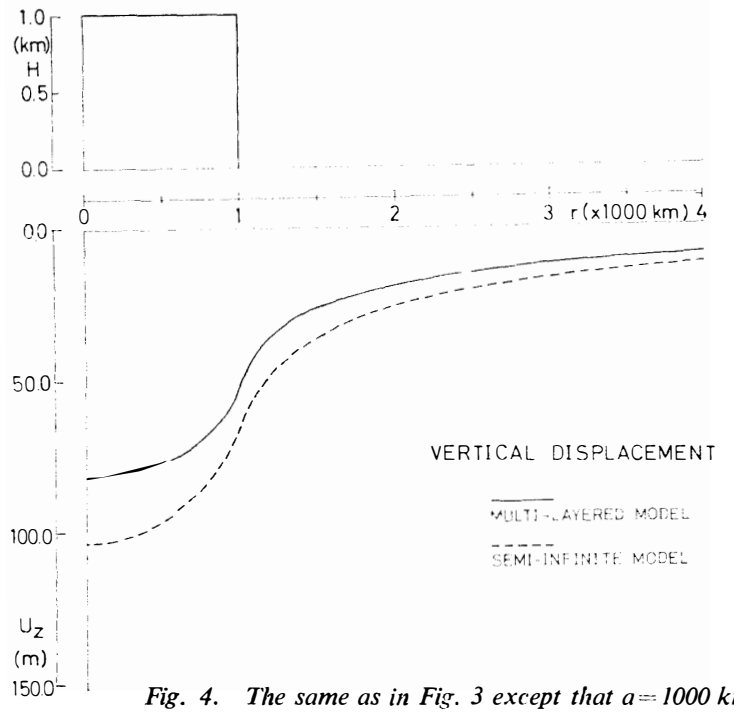

Fig. 4. The same as in Fig. 3 except that a = 1000 km.

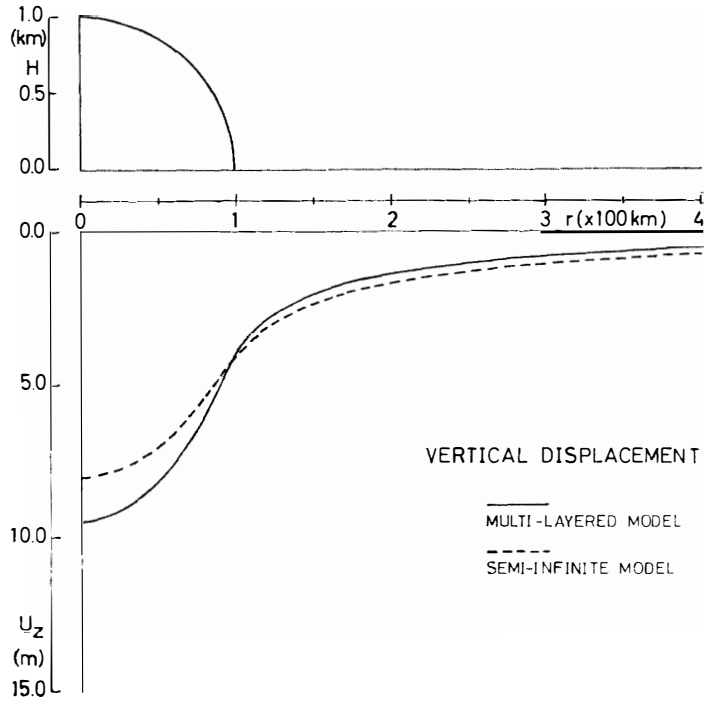

Fig. 5. Vertical displacements of the surface of the CANSD model (solid curve) and of Semi-infinite B (broken curve) for the Case II load with H=1 km and a=100 km.

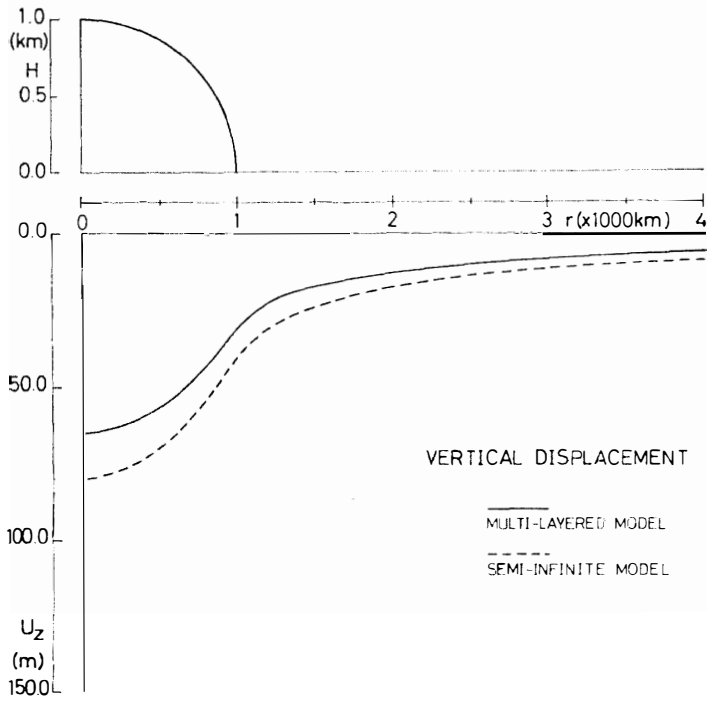

Fig. 6. The same as in Fig. 5 except that a=1000 km.

A and B are given in Table 2.

In Fig. 2 approximation function F_z (solid curve) versus $\beta=\xi a$, non-dimensionalized wave number, is shown with exact values of K_z (open circles). It can be easily seen that the simple function F_z approximates fairly well the exact values of K_z.

Vertical displacements on the surface, U_z in the load Case I, are calculated from eq. (6) for Semi-infinite B model and the CANSD model, taking the radius of load $a=100$ km. These displacements are presented in Fig. 3. As is seen in this figure, U_z for the CANSD model is larger than that for the Semi-infinite B model in the loaded region ($r<100$ km). Fig. 4 shows the vertical displacements for the same situation as in Fig. 3, except that here the radius of the ice sheet a is taken as 1000 km. In this case the vertical displacement for the Semi-infinite B model is always larger than that for the CANSD model. Similar arguments are valid in Case II, as is seen from Fig. 5 ($a=100$ km), and Fig. 6 ($a=1000$ km).

4. Discussion and Conclusion

The raised shorelines are observed at the levels of 20–30 m in the coastal snow-free areas around the Antarctic Continent (TAYLOR, 1922; NICHOLS, 1953; ADIE, 1964; YOSHIDA, 1970). The geographical feature of snow-free areas in Antarctica is the glacial landform such as glacial troughs and moraines. From these facts it is regarded that the Antarctic in the past had been covered by thicker ice sheet than the present. The ice sheet on the Antarctic Continent has retreated about at least 10 km to 100 km for the last few million years, which is estimated from the features of the continental shelf around the Antarctic Continent.

The raised shorelines in the Antarctic Continent are considered to be the results of the continental uplift after the glaciation. The static deformation described in the previous section is applied to interpret this uplift. The uplift at a certain point is calculated by the difference in vertical displacements of the surface of crust for the initial and final states of the ice sheet.

The greater part of East Antarctica is geologically characterized by a shield area and is covered with a thicker ice sheet than in West Antarctica. The radius of the ice sheet in East Antarctica is about 1700 km and the maximum thickness of it is about 4 km. A profile of the ice sheet and the Antarctic Continent along the east-west line is shown in Fig. 7 (BENTLEY, 1964). The radius of the ice sheet and its maximum thickness in East Antarctica are used for the calculation of the vertical displacement.

In Table 3, the uplift values at the point $r=1680$ km for fixed values of $a=1700$ km and $\Delta a=50$ km, with H and ΔH changing from 2 to 4 km and from 0 to 0.1 km are given for three models (Semi-infinite A, Semi-infinite B, and the CANSD) in two load cases (Cases I and II). Here H(km) is the initial thickness of the ice sheet for Case I, and the initial maximum thickness for Case II, and ΔH(km) is the decrease

in H at the final state. Also a is the initial radius of the ice sheet and Δa is the decrease in a at the final state.

The uplift values of the Semi-infinite A model in Table 3 are larger than 30 m for the resonable values of H and ΔH. This indicates that the Semi-infinite A model is not adequate to represent the crust and mantle structure beneath Antarctica.

To explain the observed fact of 20–30 m in uplift and 10–100 km in retreat, the present elasticity study gives two appropriate models:

$$\text{for Case I} \ldots H=2.0 \text{ km}, \quad H=0-0.1 \text{ km},$$

$$\text{for Case II} \ldots H=4.0 \text{ km}, \quad H=0-0.1 \text{ km}.$$

The uplift versus r (distance from the center of the ice sheet) is shown in Fig. 8 for Case I (upper part) and for Case II (lower part). The dotted line shows the uplift of the Semi-infinite B model and the solid one is that of CANSD. From the theoretical results as shown in Table 3 and Fig. 8, the uplift features between $r=1600$ km and 1700 km seem to be different for two types of load. If more observations of

Table 3. Uplift $\Delta U_r(m)$ at $r=1680$ km.

H(km)	ΔH(km)	Case I A*	Case I B**	Case I CANSD	Case II A*	Case II B**	Case II CANSD
4.0	0	82	48	56	39	23	19
4.0	0.1	98	57	63	50	30	23
3.0	0	61	35	42	29	17	14
3.0	0.1	79	45	49	40	23	19
2.0	0	41	23	28	20	11	9
2.0	0.1	59	33	35	31	17	14

* A denotes Semi-infinite A.
** B denotes Semi-infinite B.
$a=1700$ km, $\Delta a=50$ km for all the cases.

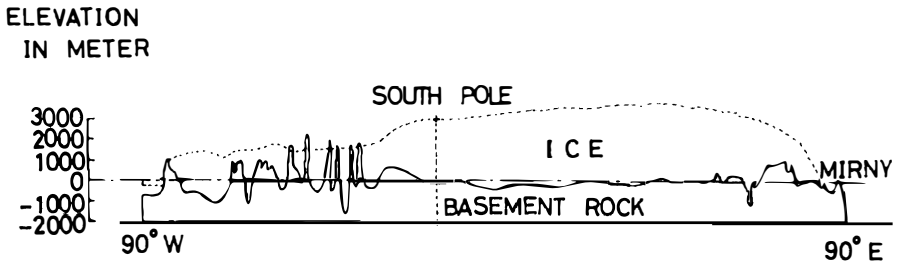

Fig. 7. Profile of vertical section of the Antarctic Continent along the longitude line of 90°E and 90°W.

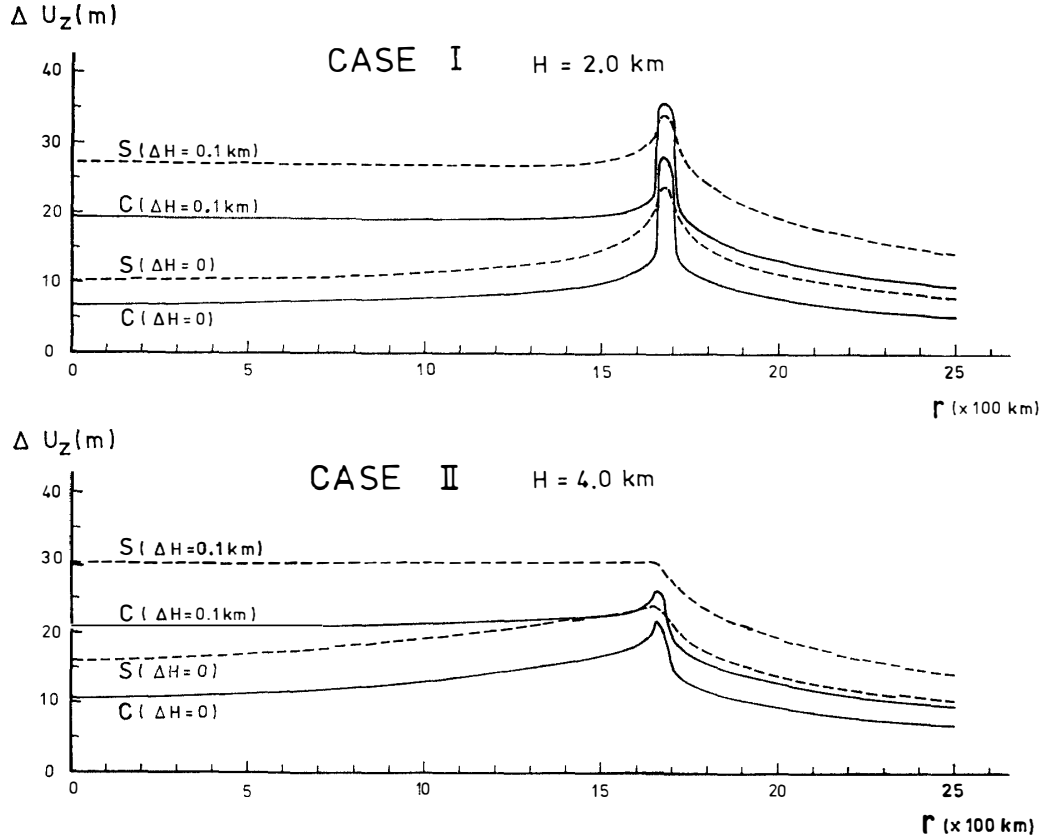

Fig. 8. Uplift ΔU_z versus r for the Case I load with $H=2$ km (upper). Uplift ΔU_z versus r for the Case II load with $H=4$ km (lower).

uplift are available for the marginal area of the Antarctic Continent, it may be possible to determine which type of load, in other words which model, can give better explanation of the uplift of the continent based on the elastic deformation theory.

The sea level change after glaciation is not discussed here, but the change is estimated as less than 10 m and the uplift is corrected by the calculation with a little larger value of Δa.

References

ADIE, R. J. (1964): Sea-level changes in the Scotia Arc and Graham Land. Antarctic Geology, ed. by R. J. ADIE. Amsterdam, North-Holland, 27–32.

BENTLEY, C. R. (1964): The structure of Antarctica and its ice cover. Research in Geophysics 2, Solid Earth and Interface Phenomena, ed. by H. ODISHAW. Cambridge, The MIT Press, 335–389.

BRUNE, J. and DORMAN, J. (1963): Seismic waves and earth structure in the Canadian shield. Bull. Seismol. Soc. Am., **53**, 167–209.

MATSU'URA M. and SATO, R. (1975): Static deformation due to the fault spreading over several layers in a multi-layered medium. Part II: Strain and tilt. J. Phys. Earth, **23**, 1–29.

NICHOLS, R. L. (1953): Geomorphology of Marguerite Bay, Palmer Peninsula, Antarctica. Washington, Office of Naval Res., 151 p. (Ronne Antarct. Res. Exped., Tech. Rep., **12**).

SATO, R. (1971): Crustal deformation due to dislocation in a multilayered medium. J. Phys. Earth, **19**, 31–46.

SATO, R. and MATSU'URA, M. (1973): Static deformations due to the fault spreading over several layers in a multi-layered medium. Part I: Displacement. J. Phys. Earth, **21**, 227–249.

TAYLOR, G. (1922): The Physiography of the McMurdo Sound and Granite Harbour Region. British Antarctic (Terra Nova) Expedition, 1910–1913. London, Harrison, 246 p.

SNEDDON, I. N. (1951): Fourier Transforms. New York, McGraw-Hill, 542 p.

YOSHIDA, Y. (1971): Higashi Nankyoku Purinsu Orafu Kaigan no ryûki teisen to enko (Raised shorelines and saline lakes in Prince Olav Coast, East Antarctica). Gendai no Chirigaku (Modern Geography), Kokin Shoin, 93–118.

(Received February 10, 1979; Revised manuscript received June 4, 1979)

Appendix

In Section 2, integral representations of the surface displacements are given by eq. (1) as follows,

$$\begin{aligned} U_r &= u_r(z=0) = -\frac{1}{2\mu_1}\int_0^\infty K_r(\xi)W^*(\xi)J_1(\xi r)d\xi, \\ U_z &= u_z(z=0) = \frac{1}{2\mu_1}\int_0^\infty K_z(\xi)W^*(\xi)J_0(\xi r)d\xi. \end{aligned} \tag{1}$$

The functions $K_r(\xi)$ and $K_z(\xi)$ are

$$\begin{aligned} K_r(\xi) &= \{(P_{14}+P_{24})(P_{32}+P_{42})-(P_{34}+P_{44})(P_{12}+P_{22})\}/\Delta, \\ K_z(\xi) &= -\{(P_{14}+P_{24})(P_{31}+P_{41})-(P_{34}+P_{44})(P_{11}+P_{21})\}/\Delta, \end{aligned} \tag{A.1}$$

with

$$\Delta=(P_{11}+P_{21})(P_{32}+P_{42})-(P_{31}+P_{41})(P_{12}+P_{22}), \tag{A.2}$$

where the matrix $[P]$ whose elements are P_{ij} is the same as that in the paper by SATO (1971), and is reproduced here as

$$[P]=[E_{n+1}]^{-1}[a_n^*][a_{n-1}^*]\cdots[a_1^*], \tag{A.3}$$

with

$$[E_{n+1}]^{-1}=\begin{bmatrix} 1, & 0, & 0, & 0 \\ 0, & -(1-\alpha_{n+1}), & (2-\alpha_{n+1}), & 0 \\ -1, & 0, & 0, & 1 \\ 0, & 1, & -1, & 0 \end{bmatrix}, \tag{A.4}$$

$$[a_j^*]=\begin{bmatrix} 1+\alpha_j\beta_jT_j, & -(1-\alpha_j)T_j-\alpha_j\beta_j, & (2-\alpha_j)T_j+\alpha_j\beta_j, & -\alpha_j\beta_jT_j \\ \alpha_j\beta_j-(1-\alpha_j)T_j, & 1-\alpha_j\beta_jT_j, & \alpha_j\beta_jT_j, & -\alpha_j\beta_j+(2-\alpha_j)T_j \\ \delta_j(\alpha_j\beta_j+\alpha_jT_j), & -\delta_j\alpha_j\beta_jT_j, & \delta_j(1+\alpha_j\beta_jT_j), & \delta_j\{(1-\alpha_j)T_j-\alpha_j\beta_j\} \\ \delta_j\alpha_j\beta_jT_j, & \delta_j(\alpha_jT_j-\alpha_j\beta_j), & \delta_j\{(1-\alpha_j)T_j+\alpha_j\beta_j\}, & \delta_j(1-\alpha_j\beta_jT_j) \end{bmatrix}, \tag{A.5}$$

and

$$\alpha_j=(\lambda_j+\mu_j)/(\lambda_j+2\mu_j), \quad \delta_j=\mu_j/\mu_{j+1}, \quad \beta_j=\xi d_j, \quad T_j=\tanh \beta_j, \tag{A.6}$$

λ_j and μ_j being Lamé's elastic constants, and d_j is the thickness of the j-th layer.

For the case of a semi-infinite medium, we can put $n=0$ in the above expressions. Then by simple calculation we can get

$$[P]=[E_1]^{-1}=\begin{bmatrix} 1, & 0, & 0, & 0 \\ 0, & -(1-\alpha_1), & (2-\alpha_1), & 0 \\ -1, & 0, & 0, & 1 \\ 0, & 1, & -1, & 0 \end{bmatrix} \tag{A.7}$$

and

$$\begin{aligned} &\Delta=\alpha_1, \\ &K_r(\xi)=(1-\alpha_1)/\alpha_1, \\ &K_z(\xi)=1/\alpha_1. \end{aligned} \tag{A.8}$$

Suffix 1 in the above two equations denotes the semi-infinite medium. This result for a semi-infinite medium is derived in a different way in the book by SNEDDON (1951).